




Cite this: *Chem. Commun.*, 2020, 56, 9655

Received 5th April 2020,  
Accepted 13th July 2020

DOI: 10.1039/d0cc02465a

rsc.li/chemcomm

# Longitudinal shape evolution of Ag<sub>2</sub>S nanoparticles from nanospheres, rhombic dodecahedrons, nanorods, to nanocubes†

Hyunmi Doh,‡ Wonseok Lee,‡ Yunmo Sung and Sungjee Kim \*

**Longitudinal shape evolution of Ag<sub>2</sub>S nanoparticles is reported. Initially 9 nm nanospheres turn into faceted rhombic dodecahedrons and elongate to minimize surface energy. The elongated rhombic dodecahedrons show oriented attachments to  $\langle -104 \rangle$  directions sequentially yielding dimers, linear oligomers, and nanorods. Lateral sides of nanorods fuse to thermodynamically stable nanocubes upon ripening.**

Silver sulfide (Ag<sub>2</sub>S) nanoparticles (NPs) constitute a new class of nanomaterials that have narrow band gap and that include no heavy metal ions such as cadmium or lead. Ag<sub>2</sub>S NPs can emit at infrared wavelengths, and therefore show promise as biocompatible imaging probes for deep tissue or highly-scattering environments such as the brain.<sup>1,2</sup> They are also applicable to environmentally-benign photocatalysts and optoelectronic device materials.<sup>3–7</sup>

NPs of different shapes often show very disparate properties which include absorption, polarization, and catalytic activities because they have different electronic structures depending on the shapes and also expose different crystal facets.<sup>8–11</sup> Various shaped Ag<sub>2</sub>S NPs have been synthesized, which encompass spheres, faceted shapes, rods, and cubes.<sup>12–17</sup> Ag<sub>2</sub>S NP shapes are typically controlled by the reaction temperature, precursor type, cation to anion precursor stoichiometry, and kinds and amounts of structure-directing agents such as alkyl amines. For micron-sized crystals, Ag<sub>2</sub>S rhombic dodecahedral crystals and nanowires have been reported.<sup>14</sup> However, shape evolution of nano-sized Ag<sub>2</sub>S crystals and underlying shape conversion mechanisms have not been fully studied. Herein, we report longitudinal synthesis of various shaped Ag<sub>2</sub>S NPs from nanospheres to faceted pseudo rhombic dodecahedral nanocrystals (DHNCs), nanorods (NRs), and finally to nanocubes (Scheme 1).

All the NPs, throughout the shapes, showed the monoclinic acanthite Ag<sub>2</sub>S crystal structures ( $a = 4.23 \text{ \AA}$ ,  $b = 6.93 \text{ \AA}$ ,  $c = 9.53 \text{ \AA}$ ,  $\alpha = 90^\circ$ ,  $\beta = 125.48^\circ$  and  $\gamma = 90^\circ$ ). The Ag<sub>2</sub>S NP shape evolution was followed by TEM, which revealed NP fusions by facet to facet to be the major process for the shape conversions. The shape evolutions from DHNCs to NRs and from NRs to cubes were proceeded through the oriented attachment of NPs along the  $(-104)$  planes and  $(-110)$  planes of acanthite Ag<sub>2</sub>S. The arrangements of Ag and S ions and crystallographic information of Ag<sub>2</sub>S DHNC are illustrated in Scheme 1.

We have previously reported size-controlled synthesis of Ag<sub>2</sub>S nanospheres, where separately pre-activated Ag and S precursors were mixed to produce Ag<sub>2</sub>S NPs and the Ag to S precursor ratio determined the size.<sup>18</sup> Similar to the Ag<sub>2</sub>S NP synthesis, Ag precursor solution was prepared by dissolving AgNO<sub>3</sub> in toluene with octylamine and S precursor solution was prepared by dissolving S powder in toluene (details in ESI†). For successful reaction, the precursors must be totally dissolved separately for >1 h by rigorous stirring before mixing. The Ag and S precursors were mixed at 60 °C, which immediately yielded nucleation and growth to Ag<sub>2</sub>S nanospheres. The reaction mixture was kept stirred at 60 °C. The Ag<sub>2</sub>S nanospheres slightly grew and began to develop facets to DHNCs which



**Scheme 1** (a) Sequential shape evolution of Ag<sub>2</sub>S NPs from nanospheres to DHNCs, NRs, and finally to nanocubes. (b) A representative TEM image of a Ag<sub>2</sub>S DHNC. (c) The arrangement of Ag and S ions in acanthite Ag<sub>2</sub>S DHNC and assignment of its contour planes (not in scale). (d) Sketch showing some crystal facets of a Ag<sub>2</sub>S DHNC when projected down to the [020] orientation. (e) Sketch showing representative Ag<sub>2</sub>S DHNC facets.

Department of Chemistry, Pohang University of Science and Technology,  
Cheongam-ro 77, Nam-Gu, Pohang, 37673, South Korea.

E-mail: sungjee@postech.ac.kr; Tel: +82-54-279-1494

† Electronic supplementary information (ESI) available. See DOI: 10.1039/d0cc02465a

‡ These authors contributed equally.



Fig. 1 TEM images of  $\text{Ag}_2\text{S}$  NPs obtained at different time points: (a) 2 h, (b) 6 h, (c) 24 h, (d) 30 h, and (e) 72 h (all the scale bars 50 nm).

acted as an important role for further shape evolution. DHNCs fused each other to form NRs, and NRs in turn fused each other laterally finally to yield nanocubes.

The  $\text{Ag}_2\text{S}$  NPs at different reaction times were observed using TEM (Fig. 1). At 2 h, slightly faceted quasi-spherical NPs appeared and the NPs showed the average diameter  $8.8 \pm 1.3$  nm (Fig. 1a). Energy dispersive spectrometry (EDS) returned Ag/S ratios of 1.88 for  $\text{Ag}_2\text{S}$  nanospheres, indicating that the surface of  $\text{Ag}_2\text{S}$  nanospheres is predominantly comprised of S ions (Table S1, ESI<sup>†</sup>). The NPs slightly grew in size and facets were more developed over time. At 6 h of reaction, the size increased to  $10.6 \pm 0.7$  nm (Fig. 1b). The facet development resulted in NPs of elongated DHNCs at 24 h. The DHNCs showed the average dimensions of  $\sim 15$  nm on the long side and  $\sim 11$  nm on the short (Fig. 1c). As reaction time increased, the products became increasingly anisotropic. After 30 h the product was rod-shaped with the long axis of 25 nm to 100 nm and short axis  $\sim 12$  nm (Fig. 1d). The final product of the reaction time over 72 h was nanocubes of tens of nm in size ranging from 20 nm to 100 nm (Fig. 1e). TEM images of lower magnifications show larger numbers of  $\text{Ag}_2\text{S}$  NPs of homogeneous shapes (Fig. S1, ESI<sup>†</sup>).

The different products by varying reaction times can be understood by the sequential evolution from the initial nanospheres to facet development, facet elongation, and fusions by oriented attachments to NRs and finally to thermodynamically stable nanocubes. At 24 h, DHNCs showed well-developed faceted shapes (Fig. 2a). In acanthite  $\text{Ag}_2\text{S}$  lattice, S ions comprise pseudo body-centered cubic (bcc) anion framework which can be considered as a slightly distorted bcc atomic arrangement.<sup>19</sup> Our reaction uses S-rich reaction condition ( $\text{Ag}/\text{S} = 0.1$ ) which introduced S-rich surfaces. The S-rich condition is considered to drive the NP shape evolution. DHNCs are enclosed by  $\{110\}$  facets of bcc S ion subunits. Within a DHNC, further facet redistribution occurred to flattened DHNCs by ripening, which reduced the symmetry of rhombic dodecahedra and resulted in the difference in lengths between the long and short sides within a DHNC by as much as 5 nm. When the facet elongation had proceeded to the degree that the longer side reached  $\sim 15$  nm, oriented attachments or fusions of the elongated DHNCs to the  $\langle -104 \rangle$  direction were promoted. During the early stage of

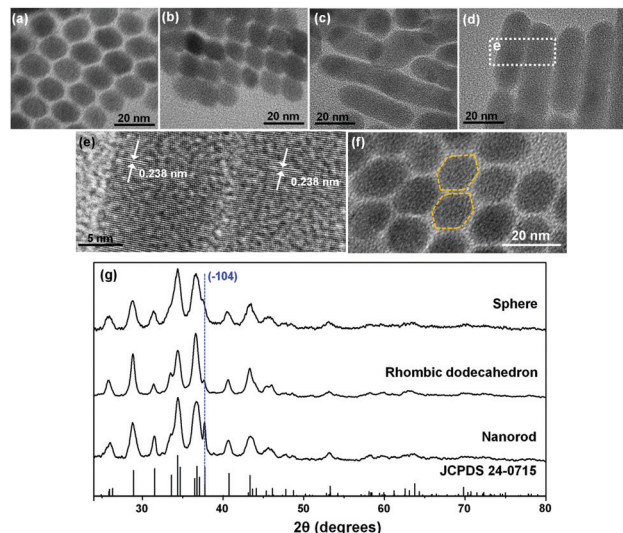


Fig. 2 TEM images of  $\text{Ag}_2\text{S}$  NPs obtained at 24 h: (a) DHNCs, (b) nanodumbbells, (c) NRs. TEM image of  $\text{Ag}_2\text{S}$  NPs obtained at 30 h: (d) NRs, HRTEM image of the dotted box as (e), showing  $d$ -spacing of  $\langle -104 \rangle$  crystal facet. (f) Representative TEM image of  $\text{Ag}_2\text{S}$  DHNCs facing each other along the  $\langle -104 \rangle$  planes, (g) XRD data of different shape of NPs.

such fusions, two slightly elongated DHNCs fused together to form nanodumbbells (Fig. 2b). After further prolonging reaction time the number of fused dodecahedrons in NP ensemble increased, and the lateral sides of nanodumbbells rapidly flattened and formed NRs (Fig. 2c). The NRs often showed winding shapes, presumably due to fusion of different-sized DHNCs (Fig. 2c). However, reaction for 30 h allowed enough time for surface-energy minimization, so the twisted shapes straightened (Fig. 2d) that had highly-crystalline internal structures (Fig. 2e). The  $\text{Ag}_2\text{S}$  NRs had the lateral width of  $11.8 \pm 1.1$  nm, which matches the diagonal distance of  $11.5 \pm 2.6$  nm in the aligned DHNCs. This corroborates the hypothesis that DHNCs coalesced at the facing  $\langle -104 \rangle$  facets.

The  $\text{Ag}_2\text{S}$  anionic crystal structure was considered as a bcc composed of a supercell that consists of multiple acanthite  $\text{Ag}_2\text{S}$  unit cells. In the bcc configuration, the rhombic dodecahedron is enclosed by  $\{110\}$  planes.  $\langle -104 \rangle$ ,  $\{024\}$ ,  $\{0-24\}$ ,  $\langle -1-12 \rangle$ ,  $\langle -112 \rangle$ , and  $\{020\}$  planes of acanthite  $\text{Ag}_2\text{S}$  comprise the planes of bcc  $\{110\}$  of the anionic supercell structure (Scheme 1). When the  $\langle -104 \rangle$  and  $\langle 10-4 \rangle$  planes are positioned as the top and bottom, the eight facets near the octahedral sites are constructed by the  $\{024\}$ ,  $\{0-24\}$ ,  $\langle -1-12 \rangle$ , and  $\langle -112 \rangle$  planes. The four equatorial faces are assigned to  $\langle -104 \rangle$  and  $\{020\}$ . Fig. 2f shows a TEM image where two DHNCs can be found facing each other along the  $\langle -104 \rangle$  axes. As the visual aid, the contours of two DHNCs were provided by the yellow dotted line. To further confirm the crystal facets that involve fusions from DHNCs to NRs and also from NRs to nanocubes, HR-TEM images were obtained for intermediates in transitions during the shape evolution. The initial  $\text{Ag}_2\text{S}$  DHNCs clearly revealed  $\langle -104 \rangle$  facets and well-developed  $(0-22)$  fringes (Fig. S2, ESI<sup>†</sup>). After 12 h reaction, it was observed that some of  $\text{Ag}_2\text{S}$  DHNCs started to merge to each other along the  $\langle -104 \rangle$

facets and  $\text{Ag}_2\text{S}$  nanodumbbells were formed (Fig. S3, ESI<sup>†</sup>). When the reaction was performed for 24 h,  $\text{Ag}_2\text{S}$  nanodumbbells were grown to rod shape revealing  $(-104)$  and  $(-122)$  planes (Fig. S4, ESI<sup>†</sup>). After further reaction,  $\text{Ag}_2\text{S}$  NRs were fused with each other through lateral  $(-110)$  planes which are almost perpendicular to the  $(-104)$  planes (Fig. S5, ESI<sup>†</sup>). The thickness of the fused NRs was 23.8 nm on average which is near to the twice of the thickness of NRs. Fused  $\text{Ag}_2\text{S}$  NRs developed into a plate-like structure where the lattice fringes corresponding to  $(0-22)$  and  $(-104)$  planes were simultaneously resolved (Fig. S6, ESI<sup>†</sup>). These plate-like structures are further evolved into  $\text{Ag}_2\text{S}$  nanocubes possibly through oriented attachments.

XRD characterizations (Fig. 2g) indicate that all the initial  $\text{Ag}_2\text{S}$  nanospheres, DHNCs, and NRs share the acanthite crystal structure (JCPDS 24-0715); this match further corroborates the hypothesis of sequential transition of facet development, elongation, and oriented attachments. As the transition proceeded,  $(-104)$  peak at the  $2\theta = 37^\circ$  grew notably. This peak was barely resolvable in XRD spectra of the initial  $\text{Ag}_2\text{S}$  nanospheres, but it stood out for the DHNCs and became quite dominant for the  $\text{Ag}_2\text{S}$  NRs. This trend suggests that the  $\text{Ag}_2\text{S}$  NRs grow in the  $\langle -104 \rangle$  direction. Lattice fringes under HR-TEM of  $\text{Ag}_2\text{S}$  NRs (Fig. 2e) confirm that the crystal growth occurs in the  $\{-104\}$  plane. Accordingly,  $\text{Ag}_2\text{S}$  nanodumbbell intermediates showed the fusion of  $\{-104\}$  planes.  $\{-104\}$  planes do not meet the two to one silver to sulfur stoichiometry and are therefore quite polar and thus may provide strong inter-facial attractions during the coalescence of DHNCs. HR-TEM revealed no noticeable stacking faults or twinning faces within the  $\text{Ag}_2\text{S}$  NRs. This uniformity also suggests complete rearrangement and ripening.

$\text{Ag}_2\text{S}$  nanocubes (Fig. 3a and b) formed after reaction for 72 h. Their size was typically tens of nanometers, which is comparable to the lengths of  $\text{Ag}_2\text{S}$  NRs. Side-by-side oriented attachments of NRs are considered to yield the nanocubes. The nanocubes were highly crystalline; some lattice fringes under the HR-TEM images could be assigned to  $(-110)$ ,  $(-104)$  and  $(0-22)$  planes (Fig. 3b–d). XRD confirmed the acanthite  $\text{Ag}_2\text{S}$  structure (JCPDS 24-0715) (Fig. 3e). The XRD patterns of nanocubes match well with acanthite  $\text{Ag}_2\text{S}$  and exhibited sharper diffraction features than those of spheres, dodecahedrons and rods due to large particle size.

In many cases, use of excess of one precursor over the other has been exploited to produce anisotropic NPs such as CdSe NRs and ZnS NRs.<sup>20,21</sup> Introduction of structure-directing agents have been also widely used.<sup>22</sup> Such unbalanced introduction of precursors or contrasting affinity of structure-directing agents toward different crystal facets result in the development of particular crystal facets, which then promote the growth in a particular direction and yield anisotropic shapes. To the contrary, our  $\text{Ag}_2\text{S}$  NPs showed the unique shape evolution by multi-step fusions among NPs: initially isotropic  $\text{Ag}_2\text{S}$  NPs to faceted DHNCs, dimers (nanodumbbells), linear oligomers of the elongated DHNCs, side-smoothened NRs, to nanocubes.

Synthesized using S-rich precursor condition, the initial  $\text{Ag}_2\text{S}$  nanospheres mostly have sulfur atoms on the surfaces.



Fig. 3 (a) TEM image of  $\text{Ag}_2\text{S}$  nanocubes obtained at 72 h and (b–d) their HR-TEM images showing  $d$ -spacing of  $(-110)$ ,  $(-104)$ , and  $(0-22)$  crystal facets. (e) XRD pattern of the  $\text{Ag}_2\text{S}$  nanocubes.

Each surface sulfur atom is bonded to two ammonium ions, and the whole sulfur–ammonium ion complexes act as a L-type ligand and can be quite labile as on and off from the surface.<sup>23</sup> Such mobility of surface adatoms (as a complex with ligated ligands) is considered to have facilitated the  $\text{Ag}_2\text{S}$  NP shape evolutions. As the complex which consists of a sulfur atom and two ammonium ions migrate from one NP facet to another facet of neighboring NPs and/or move away from the facets, the interfacing facets may have right surface stoichiometry to get fused each other. Such migrations may have also provided the attracting forces between the facing facets. Small lattice energy of  $\text{Ag}_2\text{S}$  when compared to those of CdSe or ZnS may also have contributed to the shape evolutions as ripenings of NPs can take place with much less energy barriers.

Longitudinal shape evolution of  $\text{Ag}_2\text{S}$  NPs has been followed from  $\text{Ag}_2\text{S}$  nanospheres, DHNCs, nanodumbbells, NRs, and to  $\text{Ag}_2\text{S}$  nanocubes. S-rich surfaces have promoted the shape evolution by affording mobility in surface atoms with ligated ligands. Such mobility yielded facet development, facet elongation, coalescence by oriented attachments, NR growth, and formation of nanocubes. Facetizations to DHNCs and subsequent elongations occurred to lower the surface energy. The DHNCs fused to each other along the  $\langle -104 \rangle$  direction to dimers and linear oligomers, and with surface-ripening yielded NRs. Lateral fusions among NRs produced  $\text{Ag}_2\text{S}$  nanocubes. Such understanding in shape control mechanism can offer unique ways to produce  $\text{Ag}_2\text{S}$  NPs with the crystal facets engineered on-demand. Shape-controlled and facet-controlled  $\text{Ag}_2\text{S}$  NPs can open unprecedented opportunities for catalysts and optoelectronic devices.

This work was supported by the Samsung Research Funding & Incubation Center of Samsung Electronics under Project Number SRFC-MA1701-03.

## Conflicts of interest

There are no conflicts to declare.

## Notes and references

- 1 Y. Zhang, G. Hong, Y. Zhang, G. Chen, F. Li, H. Dai and Q. Wang, *ACS Nano*, 2012, **6**, 3695.
- 2 G. Hong, J. T. Robinson, Y. Zhang, S. Diao, A. L. Antaris, Q. Wang and H. Dai, *Angew. Chem. Int. Ed.*, 2012, **51**, 9818.
- 3 A. I. Kryukov, A. L. Stroyuk, N. N. Zin'chuk, A. V. Korzhak and S. Y. Kuchmii, *J. Mol. Catal. A: Chem.*, 2004, **221**, 209.
- 4 P. Kumari, P. Chandran and S. S. Khan, *J. Photochem. Photobiol., B*, 2014, **141**, 235.
- 5 Y. Xie, S. H. Heo, Y. N. Kim, S. H. Yoo and S. O. Cho, *Nanotechnology*, 2010, **21**, 015703.
- 6 A. Tubtintae, K. L. Wu, H. Y. Tung, M. W. Lee and G. J. Wang, *Electrochem. Commun.*, 2010, **12**, 1158.
- 7 R. Gui, H. Jin, Z. Wang and L. Tan, *Coord. Chem. Rev.*, 2015, **296**, 91.
- 8 M. H. Huang and P. H. Lin, *Adv. Funct. Mater.*, 2012, **22**, 14.
- 9 W. U. Huynh, J. J. Dittmer and A. P. Alivisatos, *Science*, 2002, **295**, 2425.
- 10 I. Gur, N. A. Fromer, C. P. Chen, A. G. Kanaras and A. P. Alivisatos, *Nano Lett.*, 2007, **7**, 409.
- 11 Y. Xia, X. Xia and H.-C. Peng, *J. Am. Chem. Soc.*, 2015, **137**, 7947.
- 12 D. Wang, C. Hao, W. Zheng, Q. Peng, T. Wang, Z. Liao, D. Yu and Y. Li, *Adv. Mater.*, 2008, **20**, 2628.
- 13 H. Liu, W. W. Hu, F. Ye, Y. L. Ding and J. Yang, *RSC Adv.*, 2013, **3**, 616.
- 14 C. Yu, M. Leng, M. Z. Liu, Y. Yu, D. Liu and C. Wang, *CrystEngComm*, 2012, **14**, 3772.
- 15 L. Dong, Y. Chu, Y. Liu and L. Li, *J. Colloid Interface Sci.*, 2008, **317**, 485.
- 16 W. P. Lim, Z. Zhang, H. Y. Low and W. S. Chin, *Angew. Chem. Int. Ed.*, 2004, **43**, 5685.
- 17 Q. Lu, F. Gao and D. Zhao, *Angew. Chem., Int. Ed.*, 2002, **41**, 1932.
- 18 H. Doh, S. Hwang and S. Kim, *Chem. Mater.*, 2016, **28**, 8123.
- 19 S. I. Sadovnikov, A. I. Gusev and A. A. Rempel, *Superlattices Microstruct.*, 2015, **83**, 35.
- 20 Z. A. Peng and X. Peng, *J. Am. Chem. Soc.*, 2002, **124**, 3343.
- 21 J. H. Yu, J. Joo, H. M. Park, S. I. Baik, Y. W. Kim, S. C. Kim and T. Hyeon, *J. Am. Chem. Soc.*, 2005, **127**, 5662.
- 22 M. Rycenga, C. M. Cobley, J. Zeng, W. Li, C. H. Moran, Q. Zhang, D. Qin and Y. Xia, *Chem. Rev.*, 2011, **111**, 3669.
- 23 Y. Sung, W. Lee, E. Lee, Y. H. Ko and S. Kim, unpublished work.